Thermodynamics of nanodomain formation and breakdown in scanning probe microscopy: Landau-Ginzburg-Devonshire approach

Anna N. Morozovska,[1,*,†] Eugene A. Eliseev,[2] Yulan Li,[3,‡] Sergei V. Svechnikov,[1] Peter Maksymovych,[4] V. Y. Shur,[5] Venkatraman Gopalan,[3] Long-Qing Chen,[3] and Sergei V. Kalinin[4,*,§]

[1]*Institute of Semiconductor Physics, 41 pr. Nauki, 03028 Kiev, Ukraine*

[2]*Institute for Problems of Materials Science, National Academy of Science of Ukraine, 3 Krjijanovskogo, 03142 Kiev, Ukraine*

[3]*Department of Materials Science and Engineering, Pennsylvania State University, University Park, Pennsylvania 16802, USA*

[4]*Oak Ridge National Laboratory, Oak Ridge, Tennessee 37831, USA*

[5]*Institute of Physics and Applied Mathematics, Ural State University, Ekaterinburg 620083, Russia*

(Received 24 September 2009; published 14 December 2009)

Thermodynamics of tip-induced nanodomain formation in scanning probe microscopy of ferroelectric films and crystals is studied using the analytical Landau-Ginzburg-Devonshire approach and phase-field modeling. The local redistribution of polarization induced by the biased probe apex is analyzed including the effects of polarization gradients, field dependence of dielectric properties, intrinsic domain-wall width, and film thickness. The polarization distribution inside a "subcritical" nucleus of the domain preceding the nucleation event is shown to be "soft" (i.e., smooth without domain walls) and localized below the probe, and the electrostatic field distribution is dominated by the tip. In contrast, polarization distribution inside a stable domain is "hard" (i.e., sharp contrast with delineated domain walls) and the spontaneous polarization reorientation takes place inside a localized spatial region, where the absolute value of the resulting electric field is larger than the thermodynamic coercive field. The calculated coercive biases corresponding to formation of switched domains are in a good agreement with available experimental results for typical ferroelectric materials. The microscopic origin of the observed domain-tip elongation in the region where the probe electric field is much smaller than the intrinsic coercive field is the positive depolarization field in front of the moving-counter domain wall. For infinitely thin domain wall the depolarization field outside the semiellipsoidal domain tip is always higher than the intrinsic coercive field that must initiate the local domain breakdown through the sample depth while the domain length is finite in the energetic approach evolved by Landauer and Molotskii (we refer the phenomenon as Landauer-Molotskii paradox). Our approach provides the solution of the paradox: the domain vertical growth should be accompanied by the increase in the charged domain-wall width.

DOI: 10.1103/PhysRevB.80.214110 PACS number(s): 77.80.Fm, 77.22.Ej

I. INTRODUCTION

A. Local bias-induced phase transitions by SPM

Bias-induced phase transitions and order-parameter dynamics in polar materials are a subject of substantial experimental and theoretical interest. The examples include polarization switching in ferroelectric materials with applications to information storage and memory technologies[1–3] antiferroelectric-ferroelectric phase transitions and energy storage,[4] and a broad gamut of bias-induced transitions between ergodic, nonergodic, and ferroelectric states in ferroelectric relaxors.[5] Traditionally, these phenomena are studied macroscopically using the variants of capacitance and current-detection techniques[6] or interferometric detection.[7–10] In these studies, the information on local mechanisms controlling the nucleation and initial stages of phase transformation is essentially lost, and only averaged distributions of switching parameters and activation energies can be extracted.[11–13] This limitation is common for all polar materials with reversible bias-induced transitions and extends to other systems with partially reversible and irreversible transitions, including phase-change materials,[14] electrochemical,[15] and solid-state reactions.[16]

The emergence of the scanning probe microscopy (SPM) based techniques in the last decade opens the way to concentrate an electric field within a nanoscale volume of material[17,18] thus inducing a local phase transition. This *field-localization* approach is complementary to a classical approach in nanoscience of *material confinement* (e.g., using the nanoparticles, etc) and allows studying local properties avoiding the effect of surfaces and interfaces. For ferroelectric materials, the strongly inhomogeneous electric field causes polarization reversal in the nanosized region that can be used as a functional basis of data storage[19,20] as well as a probing technique to study local mechanisms of domain nucleation, growth, and relaxation.[21–26]

In piezoresponse force spectroscopy (PFS) approach, local polarization switching is combined with the detection of electromechanical response[27] to yield the information on domain growth below the SPM tip.[28] Spatially resolved PFS was used to study polarization switching in small volumes with negligible defect concentration[29] and to map distribution of random-bond and random-field components of disorder potential[30] as well as polarization switching on a single-defect center.[31]

These experimental developments have necessitated the theoretical analysis of domain nucleation mechanisms in the field of the SPM probe on the ideal surface[32–36] and in the presence of charged defects.[37] To date, the vast majority of these studies have been performed in the rigid dielectric approximation, as summarized below.

B. Phenomenological approaches to nanoscale polarization reversal

The "rigid ferroelectric" approximation was originally employed by Landauer[38] to calculate the energy barrier for nucleation of semiellipsoidal domain in a planar capacitor under a homogeneous electric field. A similar approximation was used by Miller and Weinreich[39] to study domain-wall motion and extended by Sidorkin[40] to analyze the wall-defect interactions. Huber[41] considered the impact of electromechanical coupling on domain nucleation in a homogeneous external field. In this model, the domain walls between the regions with field-independent (i.e., rigid) spontaneous polarization $\pm P_S$ are regarded as sharp (mathematically infinitely thin). The polarization adopts its bulk value within the domains and changes stepwise at the infinitely thin domain wall between them.

This approach was utilized in a series of works by Molotskii *et al.*[32,35,42] for analyzing domain formation under the inhomogeneous electric field of a biased SPM probe. The most striking result obtained by Molotskii *et al.* is the "ferroelectric breakdown," referred to the emergence of a stable spikelike domain with submicron radius r and length l of 10–100 microns, i.e., the polarization reversal appears in the spatial region where the vanishing field of the probe is much smaller than the intrinsic coercive field. Molotskii *et al.* explained this behavior from the free-energy consideration. Within the Landauer-Molotskii (LM) thermodynamic approach, the nucleus sizes and the equilibrium radius r, and length l of semiellipsoidal domain are calculated from the free-energy excess $F(V,r,l)=F_S(r,l)+F_V(V,r,l)+F_{DL}(r,l)$, where the positive domain-wall surface energy $F_S(r,l) \sim \psi_S lr$ at $l \gg r$ (ψ_S is the surface-energy density). The Landauer depolarization-field energy $F_{DL}(r,l)$ is positive and proportional to r^4/l at $l \gg r$ and so it vanishes as $1/l$. The negative interaction energy between the probe field and the domain is $F_V(V,r,l) \sim -Vr^2 l/(\sqrt{r^2+d^2}+d)(\gamma\sqrt{r^2+d^2}+\gamma d+l)$ (γ is dielectric anisotropy factor and V is the applied bias). It is proportional to $rl/(r+l)$ when the domain radius r exceeds the characteristic size of the tip, d, so it saturates as domain length increases. The condition of negligible surface energy ($\psi_S=0$) leads to domain breakdown $l \to \infty$ even at infinitely small bias V.

This thermodynamic analysis was further developed by Morozovska *et al.*[36,43] to account for the finite electric field below the probe, surface and bulk screening, etc. In particular, this analysis allows the description of bias dependence of the saddle point on the free-energy surface $F(V,r,l)$, i.e., the activation energy for nucleation. It was found that as a function of probe bias the activation energy scales as $\sim V^{-3}$, where V is the applied bias and in this model the nucleation process is thermally activated. For typical materials parameters, the corresponding activation energies are in the 0.1–10 eV range. However, recent experimental studies have illustrated that temperature dependence of activation bias is much weaker than predicted by the rigid model;[44] similarly, the comparison between phase-field modeling and experimental measurements indicates that the switching mechanisms in PFM is close to being intrinsic.[29]

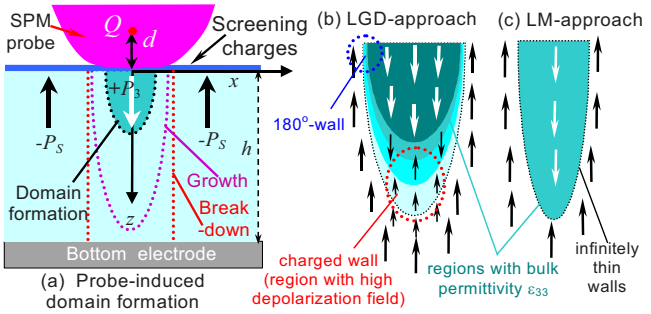

FIG. 1. (Color online) (a) Schematics of the domain nucleation caused by the strongly inhomogeneous electric field of the biased SPM probe in contact with the sample surface. [(b) and (c)] Characteristic aspects of LGD approach and rigid LM approach.

C. Polarization switching in the LGD approximation

The self-consistent description of SPM probe-induced domain formation in ferroelectrics and other ferroics requires an analytical approach based on the Landau-Ginzburg-Devonshire (LGD) thermodynamic theory. For ferroelectrics, LGD describes the dynamics of a continuous spatial distribution of the polarization vector **P** in an arbitrary electric field and the nonlinear long-range polarization interactions (correlation effects).[45,46] In this manner, the LGD approach avoids the typical limitations (sharp walls and field-independent polarization value) of the rigid ferroelectric approach [compare Figs. 1(b) and 1(c)]. Charge-neutral 180°-domain walls do not cause the depolarization electric field and usually are ultrathin. However, the charged (or counter) domain wall at the domain apex creates a strong depolarization field due to uncompensated bound charges (div $\mathbf{P} \neq 0$). The charged wall inevitably appears at the tip of the nucleating domain [Fig. 1(b)].

Polarization switching on a $BiFeO_3$ (100) ideal surface[29] and in the presence of a well-defined bicrystal grain boundary[47] was recently studied numerically using phase-field modeling. This analysis confirmed the formation of a soft subcritical nucleus below the critical bias for nucleation. Above the nucleation threshold, the formation of needlelike domains as well as domain wall broadening at the domain apex has been observed. However, the limitations of the system size for the three-dimensional phase field modeling preclude the analytical determination of the domain shape when the domain size significantly exceeds the tip size. Similarly, screening at the surface and the domain apex are difficult to access systematically.

Previously, the interaction of a ferroelectric 180°-domain wall with a strongly inhomogeneous electric field of the biased probe was studied *analytically* for a second-order ferroelectric within the LGD approach.[48] The approximate analytical expressions for the equilibrium distribution of *surface* polarization were derived from the *free-energy functional* by a direct variational method. However, *local* consideration of the electric field distribution, nonlinear and correlation effects are necessary for a reliable analysis of the polarization depth profile and the length of tip-induced domains in both first and second-order ferroelectric materials.

In this paper we adopt the local LGD-based approach for the description of the polarization dynamics in the local electric field of an SPM probe. The analytical expressions for both first- and second-order ferroelectrics are derived. Both the prenucleation and postnucleation stages are analyzed. This analysis provides insight into the effects of the intrinsic wall width, electrostatic potential distribution of the probe, ferroelectric material parameters, and the nonlinear correlation and depolarization effects on the local polarization dynamics.

II. THE PROBLEM STATEMENT

Here we study polarization switching in a uniaxial ferroelectric material. The spontaneous polarization $P_3(\mathbf{r})$ is directed along the polar axis, z. The sample is dielectrically isotropic in transverse directions, i.e., permittivities ε_{11} and ε_{22} are equal while the ε_{33} value may be different. The dependence of the in-plane polarization components on the electric field is linearized as $P_{1,2} \approx -\varepsilon_0(\varepsilon_{11}-1)\partial\varphi(\mathbf{r})/\partial x_{1,2}$. Then the problem for the electrostatic potential $\varphi(\mathbf{r})$ inside the material acquires the form

$$\varepsilon_{33}^b \frac{\partial^2\varphi}{\partial z^2} + \varepsilon_{11}\left(\frac{\partial^2\varphi}{\partial x^2} + \frac{\partial^2\varphi}{\partial y^2}\right) = \frac{1}{\varepsilon_0}\frac{\partial P_3}{\partial z}$$

$$\varphi(x,y,z=0) = V_e(x,y), \quad \varphi(x,y,z=h) = 0. \tag{1}$$

Here we introduced the dielectric permittivity of the background[49] as ε_{33}^b (typically $\varepsilon_{33}^b \leq 10$). $V_e(x,y)$ is the potential distribution at the sample surface, ε_0 is the universal dielectric constant, and h is the sample thickness.

The electrostatic potential $\varphi(\mathbf{r})$ includes the effects of the probe field as well as the depolarization field created by the bound polarization charges of the counter wall at the domain apex. The perfect screening of the depolarization field[50] outside the sample is realized by the ambient screening charges. This condition is supported both by recent experimental studies based on Kelvin probe force microscopy that demonstrate extremely small electrostatic fields above ferroelectric surfaces, indicative of almost complete screening,[51,52] density-functional theory (DFT) calculations,[53] synchrotron x-ray,[54] as well as recent studies of polarization switching in ultrathin films in ambient and in the presence of metallic electrodes.[55] Furthermore, the nucleation stage of domain formation (i.e., for small domain sizes) is primary affected by the electrostatic fields at the tip-surface junctions, for which the assumption of prescribed potential is well established.

In the effective point-charge approximation, the potential distribution produced by a SPM probe on the surface of a semi-infinite sample can be approximated as

$$V_e(\rho) \approx V\frac{d}{\sqrt{\rho^2+d^2}}, \tag{2}$$

where $\rho=\sqrt{x^2+y^2}$ is the radial coordinate, V is the applied bias, and d is the effective charge-surface separation (i.e., probe size) determined by the probe geometry [see Refs. 36, 56, and 57 and Fig. 1(a)]. The potential is normalized assuming a perfect electrical contact with the surface, $V_e(0) \approx V$. In the case of a flattened tip represented by a disk of radius R_0 in contact with a sample surface and separation $d=2R_0/\pi$ is almost independent of the film depth and its dielectric permittivity.[58]

In the framework of the LGD phenomenology, a stable or metastable spontaneous polarization distribution inside the proper ferroelectric can be found as the solution of the stationary LGD equation

$$\alpha P_3 + \beta P_3^3 + \delta P_3^5 - \xi\frac{\partial^2 P_3}{\partial z^2} - \eta\left(\frac{\partial^2 P_3}{\partial x^2} + \frac{\partial^2 P_3}{\partial y^2}\right) = -\frac{\partial\varphi}{\partial z}. \tag{3}$$

The gradient (or correlation) terms $\xi>0$ and $\eta>0$ (usually $\xi\sim\eta$), the expansion coefficient $\delta>0$ while $\beta<0$ ($\beta>0$) for first-(second-)order phase transitions. The coefficient $\alpha<0$ in the ferroelectric phase. In thin films, the coefficient α is renormalized by the elastic stress as studied in detail in Refs. 59 and 60.

The boundary conditions for the polarization distribution are

$$P_3(\rho \gg d, z<0) \to -P_S, \quad \frac{\partial P_3}{\partial z}(z=0)=0, \quad \frac{\partial P_3}{\partial z}(z=h)=0, \tag{4}$$

where P_S is the initial spontaneous polarization value. The boundary condition $\partial P_3/\partial z=0$ is called "natural"[61] and corresponds to the case when the surface-energy contribution can be neglected and hence $\lambda\to\infty$ in a more general boundary condition $P_3+\lambda(\partial P_3/\partial z)=0$. In the case of the natural boundary conditions, a constant polarization value $P_3=-P_S$ satisfies Eq. (3) at zero external bias, $V=0$. For a first-order ferroelectric, the spontaneous polarization in the bulk is $P_S^2=(\sqrt{\beta^2-4\alpha\delta}-\beta)/2\delta$ while $P_S^2=-\alpha/\beta$ for a second-order ferroelectric.[45]

III. POLARIZATION REDISTRIBUTION INDUCED BY THE PROBE BIAS: PHASE-FIELD MODELING

During polarization switching the polarization distribution is always inhomogeneous, i.e., it depends on the spatial location within the sample. In the phase-field approach,[62–64] we use the spatial distribution of local spontaneous polarization to describe a domain structure. The electric field distribution is obtained by solving the electrostatic Eq. (1). With all the important energetic contributions to the total free energy in the LGD free-energy functional $F[P_1,P_2,P_3,u_{ij}]$ as a function including the electrostatic energy, the temporal evolution of the polarization vector field and thus the domain structure is then described by the time-dependent LGD equations $\frac{\partial P_i}{\partial t}=-\Gamma\frac{\delta F}{\delta P_i}$, where Γ is the kinetic coefficient related to the domain-wall mobility. For a given initial distribution of polarization, numerical solution of time-dependent LGD equations yields the temporal and spatial evolution of polarization and thus domain switching under an external field.

The profiles of the probe-induced polarization redistribution P_3/P_S calculated numerically by phase-field modeling are shown in Figs. 2(a)–2(d). Spatial distributions of the electric field are shown in Figs. 2(e)–2(h).

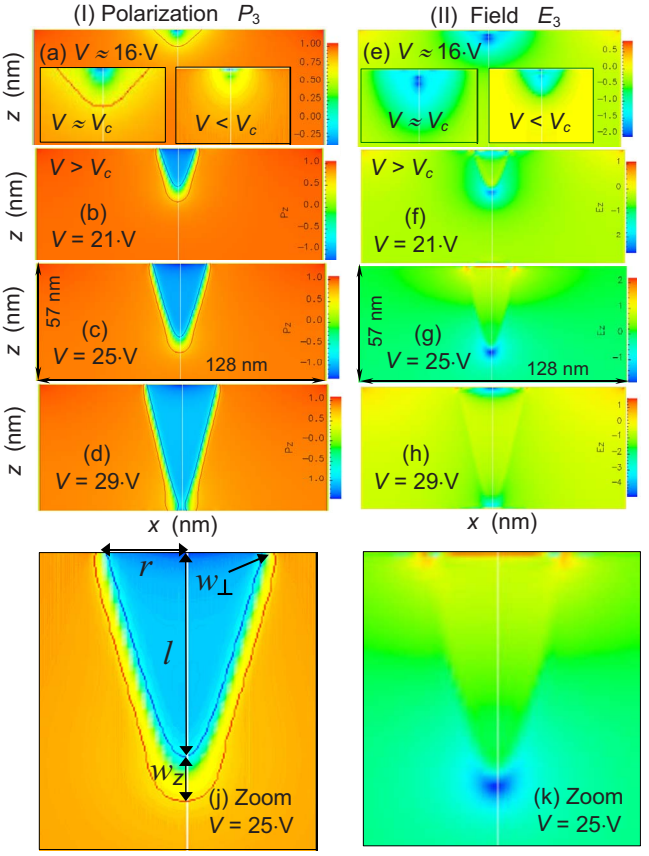

FIG. 2. (Color online) Probe-induced polarization $P_3(x,z)/P_S$ (the first row I) and electric field $E_3(x,z)$ distribution (the second row II) in $LiNbO_3$ calculated for different applied bias $V/V_0 = 16, 21, 25, 29$ (right labels). Material parameters: $\varepsilon_{33}^b = 5$, $\varepsilon_{11} = 84$, $\varepsilon_{33} = 30$, $\alpha = -1.95 \times 10^9$ m/F, $\beta = 3.61 \times 10^9$ m^5/(C^{2}F), $P_S = 0.73$ C/m^2 (Ref. 65), gradient coefficients $\eta = \xi = 10^{-9}$ SI units; effective tip-surface distance $d = 18$ nm. The simulation size is 128 nm × 128 nm × 57 nm. Plots (j) and (k) are zoomed on central parts of the plots (c) and (g).

The polarization switching is found to proceed in three stages: (1) subcritical nucleus, (2) stable domain formation and mainly vertical growth, and (3) lateral growth of the intergrown cylindrical domain. (1) At biases less than critical *nucleation bias* V_c the polarization distribution inside the subcritical domain nucleus is very smooth or "soft" with polarization maximum directly below the probe and no sharp changes like the charged domain wall appear [see right inset in Fig. 2(a)]. Depolarization field is rather weak at $V < V_c$ and thus corresponding electric field distribution is centered in the tip-surface junction area [see right inset in Fig. 2(e)]. (2) In contrast to the smooth profile of the electric field and the soft polarization distribution inside the subcritical domain nucleus, the polarization distribution inside the stable domain is "hard" but the domain-wall width is finite [compare Fig. 2(a) with Figs. 2(c) and 2(d)]. Electric field now contains significant dipolar component due to the depolarization field induced by the charge domain wall at the tip apex [compare Fig. 2(e) with Figs. 2(f) and 2(g)]. (3) As the bias increases, the domain penetrates through the sample depth and then purely radial growth proceeds [see Figs. 2(d) and 2(h)]. The depolarization field finally disappeared for a cylindrical domain.

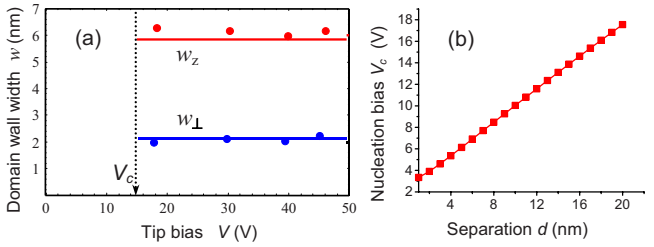

FIG. 3. (Color online) (a) Dependence of the counter domain-wall width w_z (top curve) and 180°-domain-wall width $w_\perp$ (bottom curve) vs applied bias V. Points are phase-field data, solid lines are their approximation by constant values. (b) Nucleation bias V_C vs effective tip size, d. Other parameters are the same as in Fig. 2.

Note that the condition $P_3 > P_S$ is obtained within the LGD approach with the increase in the applied bias [see scales in Figs. 2(b)–2(d)]. From Figs. 2(e)–2(h) it can be seen that the electric field is maximal outside the domain tip allowing for the strong polarizing effect (see the dark spot). In the next section we will demonstrate that the effect may be responsible for the motion of counter domain wall. Figures 2(b), 2(c), and 2(j) illustrate that the domain shape is close to prolate semiellipsoid of length l and radius r, i.e., the aspect ratio $r/l < 1$. One could also see that polarization outside the domain-wall region is almost constant.

The domain-wall *width* $w_{\perp,z}$ appeared to be orientation dependent [see Fig. 2(j)]. The width has minimal value $w_\perp$ at the surface $z = 0$ (where the 180° wall is not charged) and maximal value w_z at $z = l$, where the wall bound charge is maximal [see also schematics shown in Fig. 1(b)].

For chosen material parameters widths values are $w_\perp \approx 2$ nm and $w_z \approx 6$ nm [see Fig. 3(a)]. This result are in qualitative agreement with the results of the DFT modeling,[66] where the authors obtained that Ising-type 180° domain wall in $LiNbO_3$ is at least two times thinner that the charged wall with Neel-type characters. Note, that charged domain walls can be 10 unit cells wide in $Pb(Zr,Ti)O_3$,[67] also the walls broaden near the $LiNbO_3$ (LNO) surface allowing for stray depolarization field.[68]

For chosen parameters and $d = 18$ nm domain nucleation bias is about 15 V. It is clear from Fig. 3(b) that the nucleation bias is almost linear to effective charge-surface separation d that is proportional to the radius of the PFM tip.

IV. PROBE-INDUCED DOMAIN FORMATION: ANALYTICAL CALCULATIONS

A. Analytical expression for depolarization field

After elementary but cumbersome transformations (the details can be found in Ref. 69), exact solution of electrostatic problem (1) for the case of the probe-field radial symmetry Eq. (2) was derived as

$$E_3(\rho,z)=\int_0^\infty dkkJ_0(k\rho)\left\{\tilde{V}_e(k)\frac{\cosh[k(h-z)/\gamma_b]}{\sinh(kh/\gamma_b)}\frac{k}{\gamma_b}-\frac{\tilde{P}_3(k,z)}{\varepsilon_0\varepsilon_{33}^b}\right.$$
$$+\int_0^z dz'\frac{\tilde{P}_3(k,z')}{\varepsilon_0\varepsilon_{33}^b}\cosh\left(\frac{k}{\gamma_b}z'\right)\frac{\cosh[k(h-z)/\gamma_b]}{\sinh(kh/\gamma_b)}\frac{k}{\gamma_b}$$
$$\left.+\int_z^h dz'\frac{\tilde{P}_3(k,z')}{\varepsilon_0\varepsilon_{33}^b}\cosh\left[\frac{k}{\gamma_b}(h-z')\right]\frac{\cosh(kz/\gamma_b)}{\sinh(kh/\gamma_b)}\frac{k}{\gamma_b}\right\}, \quad (5)$$

where J_0 is the Bessel function of zero order, $\rho=\sqrt{x^2+y^2}$ is the radial coordinate, $\tilde{V}_e(k)=Vd\exp(-kd)$ is the Fourier image of $V_e(x,y)$ on transverse coordinates $\{x,y\}$, $\tilde{P}_3(k,z)$ is the Fourier image of polarization $P_3(\rho,z)$, $k=\sqrt{k_1^2+k_2^2}$ is the spatial wave-vector absolute value, and $\gamma_b=\sqrt{\varepsilon_{33}^b/\varepsilon_{11}}$ is the "bare" dielectric anisotropy factor. Further analysis of the domain formation requires the analytical description of the electric field depolarization field produced by the counter domain wall.

The spatial distribution Eq. (5) of the z component of the electric field can be represented as $E_3(\rho,z)=E_P(\rho,z)+E_W(\rho,z)$, where $E_P(\rho,z)$, is the probe field inside the sample and $E_W(\rho,z)$ is the depolarization field created by the counter domain wall. After lengthy transformations these terms were estimated from Eq. (5) as

$$E_P(\rho,z)\approx\int_0^\infty dkJ_0(k\rho)\tilde{V}_e(\mathbf{k})\frac{\cosh[k(h-z)/\gamma]}{\sinh(kh/\gamma)}\frac{k}{\gamma}=\begin{cases}\dfrac{V}{\gamma}\dfrac{(d+z/\gamma)d}{[(d+z/\gamma)^2+\rho^2]^{3/2}} & h\gg\gamma d\\ \dfrac{Vd}{2h}\left\{\dfrac{1}{\sqrt{[d-(h-z)/\gamma]^2+\rho^2}}+\dfrac{1}{\sqrt{[d+(h-z)/\gamma]^2+\rho^2}}\right\} & h\ll\gamma d\end{cases}. \quad (6)$$

The effective dielectric anisotropy factor $\gamma=\sqrt{\gamma_b^2+1/(\varepsilon_{11}\varepsilon_0\alpha)}$ originates from the linear expansion of polarization field dependence $P_3(\rho,z)\approx P_S(\rho,z)+E_3(\rho,z)/(\varepsilon_0\alpha)$, where $P_S(\rho,z)$ is the spontaneous polarization distribution. In order to derive approximate expressions the integral in Eq. (6) was expanded in the image charge series. For very thick ($h\gg\gamma d$) or ultrathin ($h\ll\gamma d$) films, the series was reduced to the first term.

When the stable domain appears, the domain wall containing the uncompensated bound electric charge with the total surface density of $\sigma_b(\mathbf{r})=2P_Sn_z(z)$ produces the additional depolarization field $E_W(\rho,z)$ [$n_z(z)$ is the outer normal to the domain boundary]. The value of $E_W(\rho,z)$ was analytically calculated using the approximation of semiellipsoidal domain with radius r, length l, and the *finite intrinsic width* $w_{\perp,z}$ of the curved domain wall.

For the case $l\ll h$ the following approximation was derived:

$$E_W(\rho,z)\approx-\int_{-1/2}^{1/2}dtE_L(\rho,z,r+tw_\perp,l+tw_z), \quad (7)$$

where the expression for the Landauer depolarization field E_L is well known as[38]

$$E_L(\rho,z,r,l)=\Delta E\begin{cases}-n_D\left(\gamma\dfrac{r}{l}\right) & \dfrac{\rho^2}{r^2}+\dfrac{z^2}{l^2}<1\\ N_D[\zeta(\rho,z),z,r,l] & \dfrac{\rho^2}{r^2}+\dfrac{z^2}{l^2}\geq 1\end{cases}. \quad (8)$$

$\Delta E=2P_S/(\varepsilon_0\varepsilon_{11}\gamma^2)$ is the field amplitude, depolarization factor n_D is (Ref. 70)

$$n_D(a)=\frac{a^2}{(1-a^2)^{3/2}}[\operatorname{arctanh}(\sqrt{1-a^2})-\sqrt{1-a^2}]. \quad (9a)$$

Approximately, $n_D(a)\sim a^2/(1+a^2)$, where $a=\gamma r/l$ is the reduced aspect ratio. Function N_D

$$N_D(\zeta,r,l)=\frac{(\gamma r/l)^2}{[1-(\gamma r/l)^2]^{3/2}}\left\{\sqrt{\frac{1-(\gamma r/l)^2}{1+\zeta\gamma^2/l^2}}\right.$$
$$-\operatorname{arctanh}\left[\sqrt{\frac{1-(\gamma r/l)^2}{1+\zeta\gamma^2/l^2}}\right]$$
$$\left.+\left[\frac{1-(\gamma r/l)^2}{1+\zeta\gamma^2/l^2}\right]^{3/2}\frac{z^2(l^2+\zeta\gamma^2)(r^2+\zeta)}{z^2(r^2+\zeta)^2\gamma^2+\rho^2(l^2+\zeta\gamma^2)^2}\right\}. \quad (9b)$$

Coordinate $\zeta(\rho,z)=0.5\{\sqrt{[r^2-\rho^2+(z^2-l^2)/\gamma^2]^2+4\rho^2z^2/\gamma^2}+\rho^2-r^2+(z^2-l^2)/\gamma^2\}$. At the domain base, $N_D(0,z=0,r,l)=-n_D(\gamma r/l)$ while at the domain tip $N_D(0,z=l,r,l)=1-n_D(\gamma r/l)$ (see supplement in Ref. 69 for details).

It is very important to notice that the field $E_W(\rho,z)$ [given by Eq. (7) for the finite wall width $w>0$] differs from the Landauer depolarization field $E_L(\rho,z)$ [given by Eq. (8) and corresponding to the case of infinitely thin domain walls with $w=0$]. The Landauer field is homogeneous inside the semiellipsoidal domain and vanishes as $(r/l)^2$ at $r/l\to 0$. However, outside the domain tip it changes the sign (allowing for the surface bound charge) and so it acts as the polarizing field that can exceed the intrinsic coercive field E_c, for the second-order ferroelectrics $E_c=P_S/(3\sqrt{3}\varepsilon_0\varepsilon_{11}\gamma^2)$ [see filled regions in Figs. 4(a) and 4(b) and compare with Figs. 2(e)–2(h) and 2(k)]. This renders the application of the Landauer model for the description of the domain growth at the latter stages not

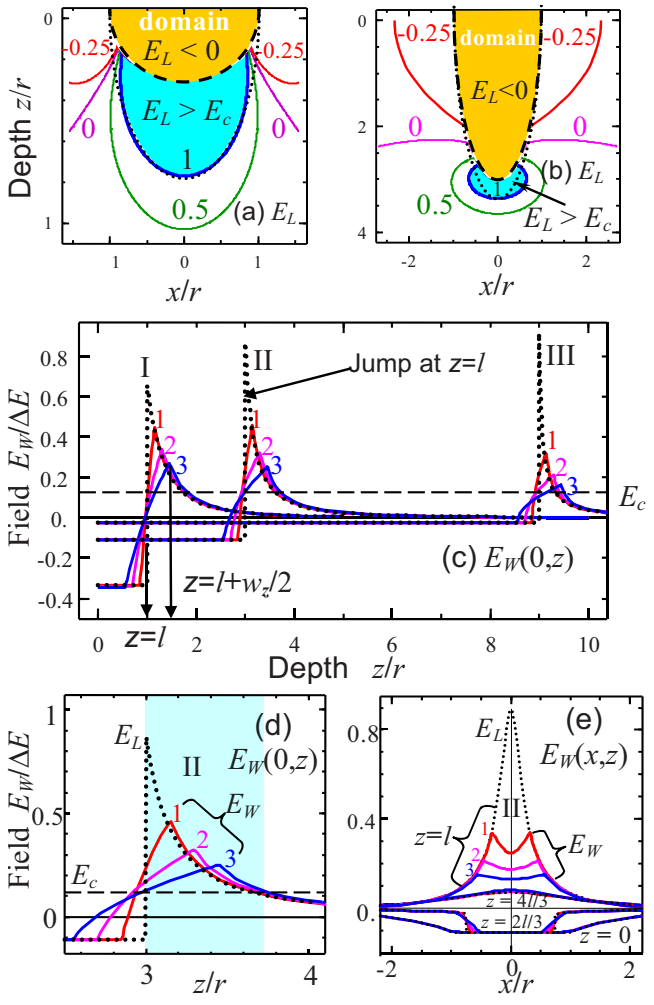

FIG. 4. (Color online) [(a) and (b)] Mechanism of domain breakdown in the case of infinitely thin counter domain wall. Constant lines of the Landauer depolarization-field ratio $E_L(\rho,z)/E_c$ for semiellipsoidal domain with radius r and length l in $LiNbO_3$ for (a) $l/r=0.3$ and (b) $l/r=3$. Dashed contour is the initial domain boundary. Filled areas indicate the region where depolarization field E_L is more than coercive field E_c. Dotted contour schematically shows the new domain boundary originated from the polarizing effect of the counter domain wall. [(c) and (d)] Depth distribution $E_W(0,z)/\Delta E$ for different aspect ratios $l/r=1,3,9$ (group of curves I, II, and III), $w_{\perp,z}=0$ (dotted curves); $w_z=3w_\perp$ and $w_\perp/r=0.1,0.2,0.3$ (solid curves 1, 2, and 3). Dashed line corresponds to coercive field E_c. (e) Cross section $E_W(x,z)/\Delta E$ for the aspect ratio $l/r=3$, different depth $z/l=0,2/3,1,4/3$; $w_z/w_\perp=3$ and $w_\perp/r=0.1,0.2,0.3$ (solid curves 1, 2, and 3) and $w_{\perp,z}=0$ (dotted curves).

self-consistent since the large field concentration at the domain apex leads to the unphysical singularity.

It directly follows from Eq. (8) that at the domain top plane $z=0$ the field $E_L(\rho,z)$ is continuous: $E_L(r-0,0)=E_L(r+0,0)=-n_D(\gamma r/l)\Delta E$ while at the domain apex the jump has appeared: $E_L(0,z=l-0)=-n_D(\gamma r/l)\Delta E$, $E_L(0,z=l+0)=[1-n_D(\gamma r/l)]\Delta E$. The jump of depolarization field $E_L(0,l)$ for the case of an infinitely thin counter domain wall is illustrated in Figs. 4(c) and 4(d) by dotted curves.

Field $E_W(0,z)$ is shown in Figs. 4(c) and 4(d) by solid curves corresponding to the increase in domain-wall width w. The field $E_W(0,z)$ is maximal at the outer boundary of the domain wall, i.e., in the point $z=l+w_z/2$, where the local breakdown is most probable. In contrast to Landauer depolarization field, the field $E_W(\rho,z)$ is continuous with the approximate expressions derived from Eq. (8): $E_W(\rho,0)\approx E_L(\rho,0)=-n_D(\gamma r/l)\Delta E$ at $\rho\leq r$, $r\gg w_\perp$, and $l\gg w_z$ [see Fig. 4(e)] while $E_W(0,l)\approx 0.5\cdot[E_L(0,l-0)+E_L(0,l+0)]$ [see Figs. 4(c) and 4(d)]. It is clear from Figs. 4(c) and 4(d) that $E_L(0,l-0)<E_W(0,l)<E_L(0,l+0)$. Analytical results shown in Figs. 4(c)–4(e) are in agreement with phase-field modeling results presented in Figs. 2(e)–2(h).

The strong *positive* depolarization field ($E_L>E_c$) in front of the infinitely thin charged domain wall causes the spontaneous increase in the domain length leading to the domain-wall breakdown into the depth of the sample (compare with the spikelike domain appearance and domain breakdown calculated within energetic LM approach). However after minimization of the corresponding LM free energy calculated for infinitely thin domain walls, the domain length appeared always finite. Thus our approach provides the solution of the Landauer-Molotskii paradox: the domain vertical growth should be accompanied by the increase in the width of the charged domain wall [see solid curves in Figs. 4(c) and 4(d)].

The width increase smears the jump of the depolarization field at the domain tip, and the domain-wall broadening and propagation is finished once the field in front of the wall becomes smaller than the coercive field. Note that mathematically Eq. (7) is similar to the *averaging of* depolarization field over the domain wall as proposed and argued by Drugard and Landauer for the flat domain wall.[71]

The transverse correlation length $w_\perp=\sqrt{\eta/(\alpha+3\beta P_S^2+5\delta P_S^4)}$ defines the finite intrinsic width of the 180°-domain wall which it is at least several lattice constants for typical values of $\xi\sim 10^{-7}\cdots 10^{-9}$ J m^3/C^2 at room temperature. For most ferroelectrics, the effective tip size $d\sim 10$ nm is typically much larger than the width $w\sim 1$ nm, this approximation is used hereinafter.

The spatial distribution of the polarization can be found as the solution of the nonlinear Eq. (3) rewritten as

$$\alpha P_3(\rho,z)+\beta P_3^3(\rho,z)+\delta P_3^5(\rho,z)-\xi\frac{\partial^2 P_3}{\partial z^2}-\eta\left(\frac{\partial^2 P_3}{\partial \rho^2}+\frac{1}{\rho}\frac{\partial P_3}{\partial \rho}\right)=E_3(\rho,z). \quad (10)$$

We emphasize that the electric field E_3 given by Eq. (5) is the sum of the probe field $E_P(\rho,z)$ and depolarization field $E_W(\rho,z)$ approximately given by Eqs. (6) and (7). The left-hand side of Eq. (10) describes the conventional ferroelectric hysteresis in the system with *spatial dispersion* (e.g., with polarization gradient). In the continuous media approximation both polarization and its second derivative are small in the immediate vicinity of domain-wall boundary since the boundary is an *inflection surface*. Under the typical condition $w(z)\ll d$, a thermodynamically stable domain-wall boundary $\rho(z)$ can be estimated from the Eq. (10) as the coercive point, i.e., under the condition $[\alpha+3\beta P_3^2(\rho,z)+5\delta P_3^4(\rho,z)]=0$ valid at coercive field: $E_3(\rho,z)=E_c$.

The intrinsic coercive field E_c is well known[72] as

$$E_c = \begin{cases} \frac{2}{3\sqrt{3}}\sqrt{-\frac{\alpha^3}{\beta}} & \text{for second order ferroelectrics} \\ \frac{2}{5}(2\beta+\sqrt{9\beta^2-20\alpha\delta})\left(\frac{2\alpha}{-3\beta-\sqrt{9\beta^2-20\alpha\delta}}\right)^{3/2} & \text{for first order ferroelectrics} \end{cases}. \quad (11)$$

Note that this analysis essentially justifies early arguments of Kolosov *et al.*[73] stating that the domain size in a PFM experiment corresponds to the region in which tip-induced field exceeds coercive field. Here we obtained a similar result but for the condition for the sum of the nascent domain depolarization field and the tip-induced field to exceed the coercive field.

B. Vertical growth of the domain in thick films

The bias dependence of the domain radius $r(V)$ at the sample surface should be determined from the equation $E_3(\rho,z)=E_c$ at $z=0$ while the domain length $l(V)$ is determined at $\rho=0$. For film with thickness $h \gg d$ and domain length $l \ll h$ we derived coupled equations for the radius r and length l bias dependences

$$\begin{cases} E_P(r,0) = E_c - E_W(r,0) \\ E_P(0,l) = E_c - E_W(0,l) \end{cases}. \quad (12)$$

Expressions for the probe field E_P and the counter domain-wall depolarization filed E_W are given by Eqs. (6) and (7). As anticipated, the domain breakdown through the sample depth ($l \to \infty$) appears under the condition $E_W > E_c$ that is true for a negligible intrinsic width $w \to 0$.

When the domain approaches the bottom electrode (opposite to the above-considered case $l \ll h$) we put $l=h$ and $E_W=0$ in Eqs. (12), and thus obtained rough estimations for the corresponding domain radius and critical bias that initiates domain intergrowth through the sample depth

$$r_{\text{int}}(h) = \begin{cases} d\sqrt{[1+(h/\gamma d)]^{4/3}-1} \sim \sqrt[3]{dh^2} & h > \gamma d \\ (h/\gamma)\sqrt{2-7(h/\gamma d)^2} \sim h & h \ll \gamma d \end{cases}, \quad (13a)$$

$$V_{\text{int}}(h) \approx \begin{cases} \gamma d\left(1+\frac{h}{\gamma d}\right)^2\left[E_c + n_D\left(\frac{\gamma r_{\text{int}}}{h}\right)\Delta E\right] \sim h^{4/3} & h > \gamma d \\ h\left[E_c + n_D\left(\frac{\gamma r_{\text{int}}}{h}\right)\Delta E\right] \sim h & h \ll \gamma d \end{cases}. \quad (13b)$$

Note that expressions (13) derived for the case of the electric excitation by the localized probe field with characteristic scale d differs from the semiempirical Kay-Dunn law[74] which stated that $r \sim h^{2/3}$ and coercive field $E_{cr} \sim h^{-2/3}$ for homogeneous external field. For films with thickness $h \gg \gamma d$, the bias dependences of the domain length $l(V)$ and radius $r(V)$ calculated from Eqs. (13) are shown in Fig. 5 for $LiNbO_3$ and Fig. 6 for typical ferroelectric materials including $LiTaO_3$ (LTO), $PbTiO_3$ (PTO), and $PbZr_{40}Ti_{60}O_3$ (PZT) in three limiting cases (i) without depolarization field, i.e., at $E_W=0$ [see dashed curves in Figs. 5 and 6]. (ii) No motion of the charged domain wall by depolarization field, i.e., $E_W(0,l)=E_L(0,l-0) \equiv -n_D(\gamma r/l)\Delta E$ [see dotted curves in Figs. 5 and 6]. (iii) The motion of the charged domain wall by the depolarization field is considered, i.e., E_W is given by Eq. (7) [see solid curves in Figs. 5 and 6].

Case (i) is possible for complete screening of the depolarization field by free carriers which immediately surround the counter domain wall. Case (ii) has unclear physical interpretation (may be strong pinning or a very fast process) and is shown in Fig. 5 for comparison only.

The calculated coercive biases $V_c \sim 1-10$ V of domain reversal are in the same range as available experimental results[28–31,76,77] but further comparison is hindered by the lack of knowledge on the exact tip geometry. At biases $V < V_c$ the domain nucleation is absent in a real time scale. Under the perfect screening of domain-wall depolarization field by free charges, the domain formation at biases $V \geq V_c$ is barrierless since a new domain appears with zero sizes $r(V_c)=l(V_c)=0$ [see dashed curves in Fig. 5(a)]. In contrast, when the motion of the charged domain wall by depolarization field is absent, activation barrier appears since unstable

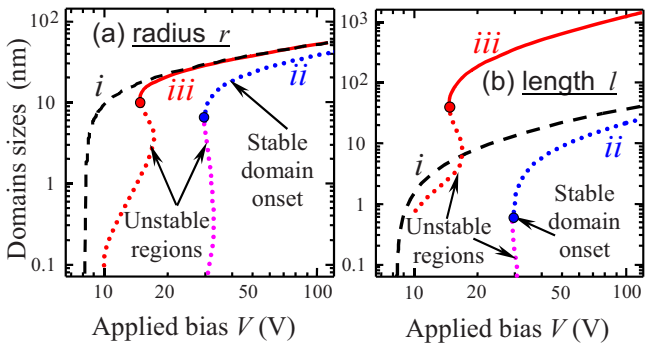

FIG. 5. (Color online) (a) Domain radius $r(V)$ and (b) length $l(V)$ bias dependence calculated within LGD approach for $LiNbO_3$ (with $\varepsilon_{11}=84$, $\varepsilon_{33}=30$, $\alpha=-1.95\times10^9$ m/F, $\beta=3.61\times10^9$ m^5/(C^{2}F), and $P_S=0.73$ C/m^2). Effective distance $d=25$ nm, $\varepsilon_{33}^b \leq 5$, sample thickness $h \to \infty$. [(a) and (b)] Solid curves are calculated from Eq. (12) for $E_W \neq 0$ given by Eq. (7) at $w_\perp=1$ nm, $w_z/w_\perp=3$ (case iii); dashed curves correspond to $E_W=0$ (case i); and dotted curves correspond to $E_W(0,l)=E_L(0,l-0)$ (case ii).

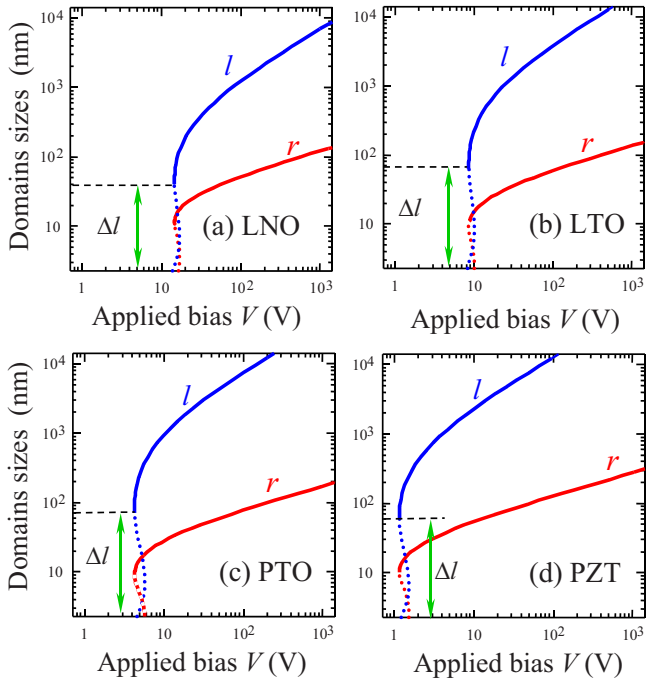

FIG. 6. (Color online) Domain length $l(V)$ and radius $r(V)$ bias dependence calculated within LGD approach for typical ferroelectric materials: LNO ($LiNbO_3$ with $\varepsilon_{11}=84$, $\varepsilon_{33}=30$, $\alpha=-1.95\times10^9$ m/F, $\beta=3.61\times10^9$ $m^5/(C^2F)$, and $P_S=0.73$ C/m^2); LTO ($LiTaO_3$ with $\varepsilon_{11}=54$, $\varepsilon_{33}=44$, $\alpha=-1.31\times10^9$ m/F, $\beta=5.04\times10^9$ $m^5/(C^2\,F)$, and $P_S=0.51$ C/m^2); PTO ($PbTiO_3$ with $\varepsilon_{11}=124$, $\varepsilon_{33}=67$, $\alpha=-3.42\times10^8$ m/F, $\beta=-2.90\times10^8$ $m^5/(C^2F)$, $\delta=1.56\times10^9$ $m^5/(C^2F)$, and $P_S=0.75$ C/m^2); PZT [$PbZr_{40}Ti_{60}O_3$ with $\varepsilon_{11}=497$, $\varepsilon_{33}=197$, $\alpha=-1.66\times10^8$ m/F, $\beta=1.44\times10^8$ $m^5/(C^2F)$, $\delta=1.14\times10^9$ $m^5/(C^2F)$, and $P_S=0.57$ C/m^2 (Ref. 75)]. Effective distance $d=25$ nm, $\varepsilon_{33}^b\leq5$, and $w_\perp=1$ nm, $w_z/w_\perp=3$, sample thickness $h\to\infty$. Solid curves are calculated from Eq. (12) for $E_W\neq0$ given by Eqs. (7).

regions appeared at the domain onset [see dotted curves at Fig. 5(a)].

Note that the behavior of the curves at sizes less that 0.8 nm shown in Fig. 5 should be ignored since for the sizes less 2–3 lattice constants, the continuous LGD approach is not expected to be applicable. However, the jumps of the domain radius Δr and length Δl up to sizes more than tens of nanometers should be interpreted as a first-order nucleation [see solid curves onset in Figs. 5 and 6]. The activation barrier disappears at coercive bias V_c.

The approximate expressions for the domain radius r, length l, bias dependences, and shape $\rho(z)$ derived from Eq. (12) are summarized in the Table I for the cases (i)–(iii). Note that the coercive bias V_c of domain formation is proportional to the intrinsic coercive field E_c given by Eq. (11). In all the cases (i)–(iii) V_c is proportional to d, the analytical result is in a perfect agreement with phase-field results presented in Fig. 3(b).

As it follows from Table I, in the absence of the domain-wall motion by the depolarization field, the domain length depends on bias as $l(V)\sim V^{1/2}$ at high voltage while the domain radius $r(V)\sim V^{1/3}$ increases more slowly than in LM approach with $l(V)\sim V$ and $r(V)\sim V^{2/3}$. If the strong positive depolarization field moves the charged domain wall, we still obtained that $r(V)\sim V^{1/3}$ but the domain length rapidly increases.

C. Lateral growth of the domain in the film

Finally, we consider the lateral growth of a cylindrical domain appeared after the domain breakdown in thin ferroelectric films. Under the condition of domain intergrowth through the film depth, the charged domain wall disappears (all walls are 180°) and so one should put $E_W=0$ in Eq. (10).

TABLE I. The domain characteristics calculated in different models.

	Intrinsic model of domain formation for thick films ($h\gg\gamma d$)		
Domain characteristics	Case (i): $E_W=0$ (complete screening of depolarization field E_W)	Case (ii): $E_W(0,l)=E_L(0,l-0)$(strong pinning or a very fast process)	Case (iii): $E_W\neq0$ (no screening of depolarization field E_W)
Coercive bias V_c	$V_c=\gamma d\cdot E_c$	$V_c=\gamma d(E_c+\Delta E)$, $\Delta E=2P_S/(\varepsilon_0\varepsilon_{11}\gamma^2)$	$\gamma dE_c<V_c<\gamma d(E_c+\Delta E)$, $\Delta E=2P_S/(\varepsilon_0\varepsilon_{11}\gamma^2)$
Domain onset at $V\to V_c$	Onset is activationless since oblate domain appears with zero sizes $r(V_c)=0$ and $l\sim r^2$	Activation barrier exists since prolate stable domain appears with nonzero sizes $l(V_c)>r(V_c)>0$	Nucleus is prolate, $r(V_c)=0$. Spikelike stable domain ($r/l\ll1$) appears after the almost first-order transition (see vertical parts of l curves)
Sizes r and l vs bias	$r(V)=d\sqrt{(V/V_c)^{2/3}-1}$, $l(V)=\gamma\cdot d(\sqrt{V/V_c}-1)$, $r^3/l^2\approx\gamma^{-2}$ at $V/V_c\gg1$	$l=\gamma d[(1+r^2/d^2)^{3/4}-1]$, $r(V\gg V_c)\sim V^{1/3}$, $l(V\gg V_c)\sim V^{1/2}$	$r(V)\approx d\sqrt{(V/V_c)^{2/3}-1}$, length $l\gg r$ is determined by f_D value
Shape at $V>V_c$	Equation for domain-wall boundary $\rho(z)=[(V/V_c)^{2/3}d^{4/3}\times(d+z/\gamma)^{2/3}-(d+z/\gamma)^2]^{1/2}$	Domain is prolate. At high voltages $V/V_c\gg1$ the invariant $r^3/l^2\approx\gamma^{-2}$ exists (compare with invariant $r^3/l^2\approx$const obtained by Molotskii[a])	Domain is strongly prolate. Domain breakdown through the sample depth ($l\to\infty$) appears under the condition infinitely thin domain-wall width $w\to0$

[a]Reference 42.

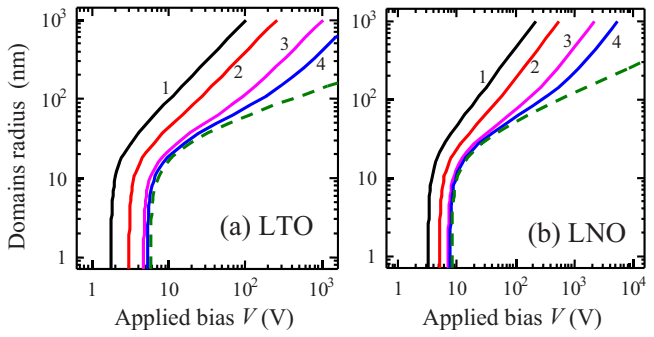

FIG. 7. (Color online) Domain radius $r(V)$ bias dependence calculated within LGD theory from for typical ferroelectric materials: (a) LTO; (b) LNO; materials parameters are listed in caption for Fig. 6; effective distance $d=25$ nm, $\varepsilon_{33}^{b}\leq 5$. Solid curves 1, 2, 3, and 4 are calculated for different film thickness h: 10, 25, 100, and 250 nm; dashed curves correspond to the dependence $r(V)=d\sqrt{(V/V_c)^{2/3}-1}$ valid in semi-infinite sample after the domain breakdown.

At finite film thickness, the electric field Eq. (6) at the sample surface acquires the form

$$E_P(\rho,z=0)=Vd\left\{\frac{d}{\gamma(d^2+\rho^2)^{3/2}}+\sum_{n=1}^{\infty}\frac{2(d+2hn/\gamma)}{\gamma[(d+2hn/\gamma)^2+\rho^2]^{3/2}}\right\}$$
$$\approx\begin{cases}\dfrac{Vd}{\gamma(d^2+\rho^2)^{1/2}}\left[\dfrac{d}{(d^2+\rho^2)}+\dfrac{\gamma}{h}\right] & h\ll\gamma d\\ \dfrac{Vd}{\gamma(d^2+\rho^2)^{3/2}}+\dfrac{2V(d+2h/\gamma)}{\gamma[(d+2h/\gamma)^2+\rho^2]^{3/2}} & h\gg\gamma d\end{cases}. \quad (14)$$

Using Eqs. (10) and (14), the domain radius dependence vs bias and film thickness should be calculated from the equation $E_P(r,0)=E_c$. The approximate analytical expressions are

$$r\approx\begin{cases}d\sqrt{(V/E_ch)^2-1} & h\ll\gamma d\\ d\sqrt{(V/\gamma E_cd)^{2/3}-1} & h\gg\gamma d\end{cases}. \quad (15)$$

Note that the dependences Eq. (15) are valid for domain lateral growth caused by the strongly inhomogeneous probe electric field in the ferroelectric film. Bias dependences $r(V)$ are shown in Fig. 7. Note that the domain radius and the coercive voltage decrease with the film thickness. Obtained numerical values are in a reasonable agreement with Cho and co-workers[78,79] data for thin LTO films.

V. DISCUSSION

As anticipated within LGD approach considering nonlinear correlation effects, the spontaneous polarization reorientation takes place inside a localized spatial region, where the absolute value of the resulting electric field is larger than the thermodynamic coercive field, i.e., $|E_3|>E_c$ while the hysteresis phenomenon appears in the range $|E_3|<E_c$. The domain breakdown through the sample depth appears for infinitely thin domain walls $[w(z)\to 0]$, i.e., in the absence of domain-wall correlation energy $(\xi,\eta\to 0)$. The microscopic origin of the domain tip elongation in the region where the probe electric field is much smaller than the intrinsic coercive field is the positive depolarization field appearing in front of the moving charged domain wall. Note that the *barrierless* hysteresis phenomenon (e.g., shown in Fig. 5 by dashed curves) calculated within the LGD approach corresponds to the *metastable state*,[6] in contrast to activation mechanism of the stable domain formation calculated within the LM energetic approach. Thus, obtained results are complementary to the energetic approach.

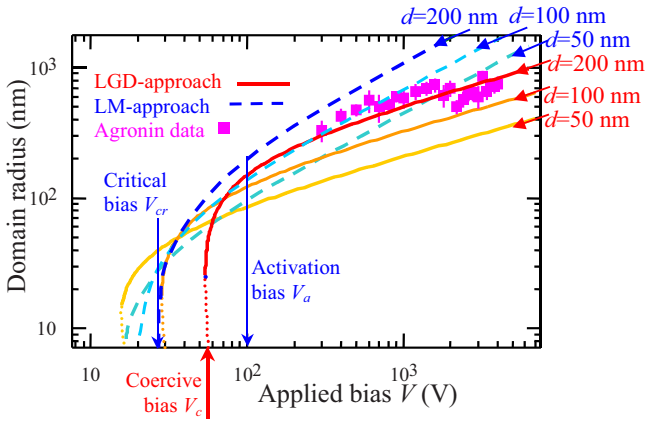

FIG. 8. (Color online) Diagram demonstrating the main features of probe-induced domain formation calculated within LGD approach (solid curves) and LM approach (dashed curves). LNO material parameters are the same as in Fig. 5, $d=50$, 100, and 200 nm (see labels near the curves), $\psi_S=0.35$ J/m^2. Squares are experimental data reported by Agronin *et al.* (Ref. 80).

As noted in the introduction, within rigid LM approach domain walls are regarded infinitely thin and polarization absolute value is constant: $-P_S$ outside and $+P_S$ inside the domain (if any). Semiellipsoidal domain radius r and length l are calculated from the free-energy excess consisting of the interaction energy, the domain-wall surface energy ψ_S and the depolarization field energy (see supplement S.3 in Refs. 32, 36, 42, and 69). Nonlinear correlation-energy contribution is absent within the rigid approximation. Within the LM approach, the depolarization field energy vanishes as $1/l$, while the interaction energy is maximal at $l\to\infty$, the condition of negligible surface energy leads to the domain breakdown $l\to\infty$ and the subsequent macroscopic region repolarization even at infinitely small bias (if only $VP_S>0$), while the hysteresis phenomena or threshold bias (saddle point) are absent 32. Under finite domain-wall energy, the critical bias V_{cr} and energetic barrier E_a of stable domain formation exist. Activation (or nucleation) bias V_a is determined from the condition $E_a(V_a)=nk_BT$, where the numerical factor $n=1,\ldots,25$. Usually $V_a\gg V_{cr}$ for thick films 36.

In Fig. 8 we compare the main features of the probe-induced domain formation calculated within intrinsic LGD approach and energetic LM approach. For consistency between the approaches we used the Zhirnov expression for the domain-wall surface energy

$$\psi_S = \sqrt{\left\{1 + \frac{2[(Q_{11}^2 + Q_{12}^2)s_{11} - 2Q_{11}Q_{12}s_{12}]}{\beta(s_{11}^2 - s_{12}^2)}\right\}\eta}\frac{(-2\alpha)^{3/2}}{3\beta}, \tag{16}$$

where Q_{ij} are electrostriction tensor and s_{ij} are elastic compliances.[59]

It is clear from the figure that both approaches fit experimental data adequately however best fitting corresponds to higher d value (about 200 nm) within LGD approach than in the LM approach (about 100 nm). However for all d values LM curve increases more rapidly with the bias increase [as $r(V) \sim V^{2/3}$] than the experimental data.[80] LGD curve increases more slowly as $r(V) \sim V^{1/3}$, which is in better agreement with the experimental data. The possible reason of the discrepancy is pinning effects not considered in LM approach and considered in some sense by LGD approach allowing for cubic nonlinearity that rules ferroelectric hysteresis.

Unfortunately, Agronin *et al.*[80] did not report neither the values of tip radius nor measured the effective tip size d. Since the size d can be increased during the tip operating (e.g., due to the tip apex erasure[81]), we treat it as a fitting parameter.

Finally, we discuss the possible role of the surface screening on nucleation process. The dominant contribution to the electrostatic fields stem from the conducting tip-surface junction, at which potential can be assumed to be well defined. At the region immediately outside tip-surface contact, the upper surface potential still was determined by function $V_e(x,y)$ while the bottom surface was regarded equipotential [see the boundary conditions to Eq. (1)]. Thus, the applicability of obtained results to the realistic tip-induced domain formation is determined from the interplay between the rate of the applied electric bias changing t_e, the formation time t_d of the domain lateral sizes, and the relaxation time t_s of the surface screening charges that is determined by their mobility. Namely, the strong inequalities should be valid $t_e \gg t_s$ and $t_e \gg t_d$. Since the value t_e can be varied in the experiment, below we estimate the ranges of t_s and t_d variation.

Formation time of the domain pattern t_d could be estimated as the domain sizes divided on the domain-wall speed v_d. In accordance with the activation-rate theory, corresponding domain nucleation time τ is determined from the equation $\tau = \tau_0 \exp(W_b/k_BT)$, where the phonon relaxation time $\tau_0 \sim 10^{-12}-10^{-13}$ s, W_b is the activation barrier. For zero external electric field the activation barriers of polarization reorientation W_b in rigid ferroelectric materials considered in the paper are extremely high. However the barrier drastically decreases up to zero when the field approaches the intrinsic coercive field. The same statement was proved for the PFM probe-induced domain formation.[48] For the considered case the thermodynamic domain-wall movement appears only when to the full electric field exceeds the intrinsic coercive field thus it is barrierless at coercive field.

In reality possible factors, which limit the domain-wall speed v_d, are the lattice pinning, pinning by defects and intrinsic velocity of phonons. The latter could be estimated as the lattice constant divided by the corresponding relaxation time τ_0, which gives $v_d \sim 40-400$ m/s. The domain-wall speed measured experimentally strongly depends on the applied electric field and varies in the range $10^{-3}-10^2$ m/s.[82,83] So the formation time of the domain with lateral sizes about 10–1000 nm could be estimated as $t_d \sim 10^{-3}-10^{-10}$ s.

The relaxation time of the surface screening charges t_s is extremely small below the conducting tip placed in the direct contact with surface [as shown in Fig. 1(a)] since here the free carriers abundant in the metal provide the immediate screening. Thus the condition $t_e \gg t_d$ is necessary for our results applicability until the domain lateral sizes is smaller than the tip-surface contact radius.

The relaxation time t_s increases when domain lateral sizes exceed the tip-surface contact radius (or such contact is absent) and typically varies in the range $10^{-3}-10^{-8}$ s depending on the ambient atmosphere (see, e.g., Refs. 36 and 84 and references therein) while for the free surface the relaxation time could be as high as 10^2 s.[52] Thus we could conclude that the condition $t_e \gg t_s$ is necessary for our results applicability when the domain lateral sizes is much greater than the tip-surface contact radius. Note that both inequalities $t_e \gg t_s$ and $t_e \gg t_d$ can be satisfied simultaneously for rather moderate values of the applied electric bias changing rate t_e.

VI. SUMMARY

The mechanism of the bias-induced phase transitions and domain formation in the localized electric field of an SPM tip is analyzed using the analytical Landau-Ginzburg-Devonshire theory and numerical phase-field modeling. This combined approach takes into account the intrinsic domain-wall width and nonlinear correlation effects. Obtained results provide insight how the polarization redistribution depends on the gradient energy, nonlinear correlation and depolarization effects, distribution of the probe's electrostatic potential, and ferroelectric properties of the material.

Polarization switching is found to proceed in three stages: (1) subcritical nucleus, (2) stable domain formation and mainly vertical growth, (3) lateral growth of the intergrown cylindrical domain. Below the coercive bias, the polarization distribution inside the subcritical domain nucleus is very soft [see smooth color changes in Figs. 2(a)] with polarization maximum directly below the probe. The corresponding electric field distribution is centered in the tip-surface junction area. In contrast, the polarization distribution inside a stable domain is rather hard [see contract colors in the Figs. 2(b)–2(e)]. Electric field now contains a significant dipolar component due to the depolarization field induced by the charge domain wall at the tip apex. As bias increases, domain penetrates through the sample depth leading to purely radial growth appeared.

The corresponding coercive bias for the formation of a stable domain is in reasonable agreement with available experimental results for typical ferroelectric materials. The microscopic origin of the domain elongation in the region where the electric field of the probe is much smaller than the

intrinsic coercive field is the positive depolarization field in front of the moving charged domain wall. Domain breakdown through the sample depth occurs for infinitely thin domain walls.

Note that a high-PFM response contrast is possible when the reversed polarization value near the probe apex is essentially higher than the sample spontaneous polarization far from the probe. The condition was obtained with the increase in the applied bias. This opens a pathway for high-density data storage in ultrathin layers of ferroelectric materials with high nonlinear field and correlation effects.

ACKNOWLEDGMENTS

Research sponsored by Ministry of Science and Education of Ukraine (Grant No. UU30/004) and National Science Foundation (Grants No. DMR-0908718 and No. DMR-0820404). A.N.M. and S.V.S. gratefully acknowledge financial support from National Academy of Science of Ukraine, joint Russian-Ukrainian under Grants No. NASU N 17-Ukr_a and No. RFBR N 08-02-90434. The research is supported in part (S.V.K.) by the Division of Scientific User Facilities, U.S. DOE.

*Corresponding author.
†morozo@i.com.ua
‡Present address: Pacific Northwest National Laboratory, 902 Battelle Boulevard, P.O. Box 999, MSIN K7–90, RIchland, WA 99352, U.S.A.
§sergei2@ornl.gov

[1] R. Waser and A. Rüdiger, Nature Mater. **3**, 81 (2004).
[2] *Nanoelectronics and Information Technology*, edited by R. Waser (Wiley-VCH, Berlin, 2005).
[3] J. F. Scott, *Ferroelectric Memories* (Springer, New York, 2000).
[4] B. Neese, B. Chu, S. G. Lu, Y. Wang, E. Furman, and Q. M. Zhang, Science **321**, 821 (2008).
[5] A. A. Bokov and Z.-G. Ye, J. Mater. Sci. **41**, 31 (2006).
[6] B. Jaffe, W. R. Cook, and H. Jaffe, *Piezoelectric Ceramics* (Academic, London, New York, 1971).
[7] A. L. Kholkin, Ch. Wuthrich, D. V. Taylor, and N. Setter, Rev. Sci. Instrum. **67**, 1935 (1996).
[8] T. Maeder, P. Muralt, L. Sagalowicz, I. Reaney, M. Kohli, A. Kholkin, and N. Setter, Appl. Phys. Lett. **68**, 776 (1996).
[9] A. L. Kholkin, E. L. Colla, A. K. Tagantsev, D. V. Taylor, and N. Setter, Appl. Phys. Lett. **68**, 2577 (1996).
[10] A. L. Kholkin, K. G. Brooks, and N. Setter, Appl. Phys. Lett. **71**, 2044 (1997).
[11] Y. Ishibashi and Y. Takagi, J. Phys. Soc. Jpn. **31**, 506 (1971).
[12] M. Avrami, J. Chem. Phys. **7**, 1103 (1939).
[13] A. N. Kolmogorov, Izv. Akad. Nauk SSSR, Ser. Mat. **1**, 355 (1937).
[14] A. Pirovano, A. L. Lacaita, A. Benvenuti, F. Pellizzer, and R. Bez, IEEE Trans. Electron Devices **51**, 452 (2004).
[15] K. Terabe, T. Hasegawa, T. Nakayama, and M. Aono, Nature (London) **433**, 47 (2005).
[16] S. V. Kalinin, B. J. Rodriguez, S. Jesse, P. Maksymovych, K. Seal, M. Nikiforov, A. P. Baddorf, A. L. Kholkin, and R. Proksch, Mater. Today **11** (11), 16 (2008).
[17] G. Rosenman, P. Urenski, A. Agronin, Y. Rosenwaks, and M. Molotski, Appl. Phys. Lett. **82**, 103 (2003).
[18] P. Paruch, T. Giamarchi, T. Tybell, and J.-M. Triscone, J. Appl. Phys. **100**, 051608 (2006).
[19] C. H. Ahn, T. Tybell, L. Antognazza, K. Char, R. H. Hammond, M. R. Beasley, Ø. Fischer, and J.-M. Triscone, Science **276**, 1100 (1997).
[20] Y. Cho, S. Hashimoto, N. Odagawa, K. Tanaka, and Y. Hiranaga, Appl. Phys. Lett. **87**, 232907 (2005).
[21] K. Terabe, M. Nakamura, S. Takekawa, K. Kitamura, S. Higuchi, Y. Gotoh, and Y. Cho, Appl. Phys. Lett. **82**, 433 (2003).
[22] B. J. Rodriguez, R. J. Nemanich, A. Kingon, A. Gruverman, S. V. Kalinin, K. Terabe, X. Y. Liu, and K. Kitamura, Appl. Phys. Lett. **86**, 012906 (2005).
[23] Y. Kan, X. Lu, X. Wu, and J. Zhu, Appl. Phys. Lett. **89**, 262907 (2006).
[24] X. Liu, K. Terabe, and K. Kitamura, Phys. Scr., T **T129**, 103 (2007).
[25] Y. Kan, X. Lu, H. Bo, F. Huang, X. Wu, and J. Zhu, Appl. Phys. Lett. **91**, 132902 (2007).
[26] A. Roelofs, T. Schneller, K. Szot, and R. Waser, Appl. Phys. Lett. **81**, 5231 (2002).
[27] S. V. Kalinin, B. J. Rodriguez, S. Jesse, E. Karapetian, B. Mirman, E. A. Eliseev, and A. N. Morozovska, Annu. Rev. Mater. Res. **37**, 189 (2007).
[28] I. Bdikin, A. Kholkin, A. N. Morozovska, S. V. Svechnikov, S.-H. Kim, and S. V. Kalinin, Appl. Phys. Lett. **92**, 182909 (2008).
[29] S. V. Kalinin, B. J. Rodriguez, S. Jesse, Y. H. Chu, T. Zhao, R. Ramesh, S. Choudhury, L.-Q. Chen, E. A. Eliseev, and A. N. Morozovska, Proc. Natl. Acad. Sci. U.S.A. **104**, 20204 (2007).
[30] S. Jesse, B. J. Rodriguez, S. Choudhury, A. P. Baddorf, I. Vrejoiu, D. Hesse, M. Alexe, E. A. Eliseev, A. N. Morozovska, J. Zhang, L.-Q. Chen, and S. V. Kalinin, Nature Mater. **7**, 209 (2008).
[31] S. V. Kalinin, S. Jesse, B. J. Rodriguez, Y. H. Chu, R. Ramesh, E. A. Eliseev, and A. N. Morozovska, Phys. Rev. Lett. **100**, 155703 (2008).
[32] M. Molotskii, A. Agronin, P. Urenski, M. Shvebelman, G. Rosenman, and Y. Rosenwaks, Phys. Rev. Lett. **90**, 107601 (2003).
[33] S. V. Kalinin, A. Gruverman, B. J. Rodriguez, J. Shin, A. P. Baddorf, E. Karapetian, and M. Kachanov, J. Appl. Phys. **97**, 074305 (2005).
[34] A. Yu. Emelyanov, Phys. Rev. B **71**, 132102 (2005).
[35] M. Molotskii and M. Shvebelman, Philos. Mag. **85**, 1637 (2005).
[36] A. N. Morozovska, S. V. Svechnikov, E. A. Eliseev, S. Jesse, B. J. Rodriguez, and S. V. Kalinin, J. Appl. Phys. **102**, 114108 (2007).
[37] A. N. Morozovska, S. V. Svechnikov, E. A. Eliseev, B. J. Rodriguez, S. Jesse, and S. V. Kalinin, Phys. Rev. B **78**, 054101 (2008).
[38] R. Landauer, J. Appl. Phys. **28**, 227 (1957).

[39] R. C. Miller and G. Weinreich, Phys. Rev. **117**, 1460 (1960).
[40] A. S. Sidorkin, Ferroelectrics **150**, 313 (1993).
[41] J. E. Huber, J. Mater. Res. **21**, 557 (2006).
[42] M. Molotskii, J. Appl. Phys. **93**, 6234 (2003).
[43] A. N. Morozovska, E. A. Eliseev, and S. V. Kalinin, Appl. Phys. Lett. **89**, 192901 (2006).
[44] P. Maksymovych, S. Jesse, M. Huijben, R. Ramesh, A. N. Morozovska, S. Choudhury, L.-Q. Chen, A. P. Baddorf, and S. V. Kalinin, Phys. Rev. Lett. **102**, 017601 (2009).
[45] M. E. Lines and A. M. Glass, *Principles and Applications of Ferroelectric and Related Materials* (Clarendon, Oxford, 1977).
[46] C. H. Woo and Y. Zheng, Appl. Phys. A: Mater. Sci. Process. **91**, 59 (2008).
[47] B. J. Rodriguez, S. Choudhury, Y. H. Chu, A. Bhattacharyya, S. Jesse, K. Seal, A. P. Baddorf, R. Ramesh, L.-Q. Chen, and S. V. Kalinin, Adv. Funct. Mater. **19**, 2053 (2009).
[48] A. N. Morozovska, S. V. Kalinin, E. A. Eliseev, V. Gopalan, and S. V. Svechnikov, Phys. Rev. B **78**, 125407 (2008).
[49] A. K. Tagantsev and G. Gerra, J. Appl. Phys. **100**, 051607 (2006).
[50] R. Kretschmer and K. Binder, Phys. Rev. B **20**, 1065 (1979).
[51] S. V. Kalinin and D. A. Bonnell, Phys. Rev. B **63**, 125411 (2001).
[52] S. V. Kalinin, C. Y. Johnson, and D. A. Bonnell, J. Appl. Phys. **91**, 3816 (2002).
[53] Y. H. Shin, I. Grinberg, I. W. Chen, and A. M. Rappe, Nature (London) **449**, 881 (2007).
[54] R. V. Wang, D. D. Fong, F. Jiang, M. J. Highland, P. H. Fuoss, Carol Thompson, A. M. Kolpak, J. A. Eastman, S. K. Streiffer, A. M. Rappe, and G. B. Stephenson, Phys. Rev. Lett. **102**, 047601 (2009).
[55] A. Gruverman, J. S. Cross, and W. S. Oates, Appl. Phys. Lett. **93**, 242902 (2008).
[56] S. Gómez-Moñivas, L. S. Froufe-Perez, A. J. Caamano, and J. J. Saenz, Appl. Phys. Lett. **79**, 4048 (2001).
[57] M. Abplanalp, Ph.D. thesis, Swiss Federal Institute of Technology, 2001.
[58] A. N. Morozovska, E. A. Eliseev, and S. V. Kalinin, J. Appl. Phys. **102**, 074105 (2007).
[59] V. A. Zhirnov, Zh. Eksp. Teor. Fiz. **35**, 1175 (1958) [Sov. Phys. JETP **8**, 822 (1959)].
[60] W. Cao and L. E. Cross, Phys. Rev. B **44**, 5 (1991).
[61] G. A. Korn and T. M. Korn, *Mathematical Handbook for Scientists and Engineers* (McGraw-Hill, New York, 1961).
[62] Y. L. Li, S. Y. Hu, Z. K. Liu, and L. Q. Chen, Appl. Phys. Lett. **78**, 3878 (2001).
[63] Y. L. Li, S. Y. Hu, S. K. Liu, and L. Q. Chen, Acta Mater. **50**, 395 (2002).
[64] Sergei V. Kalinin, Anna N. Morozovska, Long Qing Chen, and Brian J. Rodriguez, Rep. Prog. Phys. (to be published).
[65] D. A. Scrymgeour, V. Gopalan, A. Itagi, A. Saxena, and P. J. Swart, Phys. Rev. B **71**, 184110 (2005).
[66] D. Lee, R. K. Behera, P. Wu, H. Xu, Y. L. Li, S. B. Sinnott, S. R. Phillpot, L. Q. Chen, and V. Gopalan, Phys. Rev. B **80**, 060102(R) (2009).
[67] C. L. Jia, S.-B. Mi, K. Urban, I. Vrejoiu, M. Alexe, and D. Hesse, Nature Mater. **7**, 57 (2008).
[68] S. Choudhury, Yulan Li, Nozomi Odagawa, Aravind Vasudevarao, L. Tian, Pavel Capek, Volkmar Dierolf, Anna N. Morozovska, Eugene A. Eliseev, Sergei Kalinin, Yasuo Cho, Longqing Chen, and Venkatraman Gopalan, J. Appl. Phys. **104**, 084107 (2008).
[69] A. N. Morozovska, E. A. Eliseev, S. V. Svechnikov, P. Maksymovych, and S. V. Kalinin, arXiv:0811.1768 (unpublished).
[70] L. D. Landau, E. M. Lifshitz, and L. P. Pitaevskii, *Electrodynamics of Continuous Media*, 2nd ed. (Butterworth-Heinemann, Oxford, 1984).
[71] M. E. Drougard and R. Landauer, J. Appl. Phys. **30**, 1663 (1959).
[72] S. Ducharme, V. M. Fridkin, A. V. Bune, S. P. Palto, L. M. Blinov, N. N. Petukhova, and S. G. Yudin, Phys. Rev. Lett. **84**, 175 (2000).
[73] O. Kolosov, A. Gruverman, J. Hatano, K. Takahashi, and H. Tokumoto, Phys. Rev. Lett. **74**, 4309 (1995).
[74] H. F. Kay and J. W. Dunn, Philos. Mag. **7**, 2027 (1962).
[75] M. J. Haun, E. Furman, S. J. Jang, and L. E. Cross, Ferroelectrics **99**, 63 (1989).
[76] P. Paruch, T. Tybell, and J.-M. Triscone, Appl. Phys. Lett. **79**, 530 (2001).
[77] C. Durkan, M. E. Welland, D. P. Chu, and P. Migliorato, Appl. Phys. Lett. **76**, 366 (2000).
[78] K. Fujimoto and Y. Cho, Appl. Phys. Lett. **83**, 5265 (2003).
[79] Y. Daimon and Y. Cho, Appl. Phys. Lett. **90**, 192906 (2007).
[80] A. Agronin, Y. Rosenwaks, and G. Rosenman, Appl. Phys. Lett. **85**, 452 (2004).
[81] L. Tian, Aravind Vasudevarao, A. N. Morozovska, E. A. Eliseev, S. V. Kalinin, and V. Gopalan, J. Appl. Phys. **104**, 074110 (2008).
[82] T. Tybell, P. Paruch, T. Giamarchi, and J.-M. Triscone, Phys. Rev. Lett. **89**, 097601 (2002).
[83] A. Gruverman, D. Wu, and J. F. Scott, Phys. Rev. Lett. **100**, 097601 (2008).
[84] V. Shur, Phase Transitions **65**, 49 (1998).